JOURNAL OF AIRCRAFT
Vol. 38, No. 1, January–February 2001

Numerical Study of a Wing-Tip Vortex Using the Euler Equations

Robert E. Spall*
Utah State University, Logan, Utah 84322-4130

The issue of excessive diffusion of wing-tip vortex calculations is addressed. In particular, a second-order accurate pressure-based finite volume algorithm was employed to solve the Euler equations for the flow over a NACA 0012 rectangular wing at an angle of attack of 5 deg. A computational mesh was constructed that allowed for very localized grid clustering about the wing tip and about the vortex centerline over arbitrary downstream distances. Comparisons with existing experimental data show that the vortex strength and core radius are well preserved at a distance of 10 chords downstream from the wing leading edge. It is concluded that by employing well-designed computational grids, second-order accurate numerical algorithms may present a viable alternative to higher-order schemes in the solution of the tip vortex problem.

Introduction

TIP vortices shed from lifting surfaces of finite span are of considerable technological importance. For example, tip vortices contribute to the induced drag of the generating surface, a situation that is exacerbated for low aspect ratio surfaces such as marine propellers. The pressure driven flow about the tip of the lifting surface also decreases the efficiency of fluid dynamic devices such as axial compressors and turbomachine blades. Vortex–structure interaction problems, such as the blade–vortex interaction that occurs when vortices shed from a helicopter rotor blade interact with a following blade, are of considerable importance; the resulting large, unsteady forces may contribute to premature blade failure. Perhaps the vortex–structure interaction problem that has received most attention is the wake–vortex problem in which trailing wing-tip vortices pose a hazard to smaller following aircraft. In fact, the Federal Aviation Administration dictates the frequency of takeoff and landing at the nation's airports by accounting for the presence and demise of these vortices. An up-to-date review of the wake–vortex problem may be found in Spalart.[1]

Of primary interest in the present work is the wake–vortex problem, and in particular, efforts at computational simulations of the tip-vortex in the near field. One of the earliest sets of calculations were those of Mansour[2] in which the thin-layer Navier–Stokes equations were solved for the flow over a low aspect ratio swept wing at a freestream Mach number of 0.8, with the turbulence viscosity computed using a two-layer Baldwin–Lomax model. Srinivasan et al.[3] also solved the thin-layer Navier–Stokes equations with a Baldwin–Lomax model for the flow over several different wings with different tip configurations. In addition to the cited viscous results, solutions to the Euler equations for subsonic and transonic flows about helicopter rotors were presented by Kramer et al.[4] (In this case, numerical dissipation provides the mechanism for vortex formation.)

The numerical results in the cited studies showed reasonable agreement with experimentally measured surface pressures, although no comparisons between numerical and experimental results were presented for the structure of the resultant tip vortices. However, with the relatively coarse grids employed, considerable differences would have been expected.

Euler solutions were also presented by Strawn[5] for the flow about a NACA 0015 wing using an unstructured, adaptive grid solver. Results were compared with the experimental data of McAlister and Takahashi[6] at distances of up to 13 chords downstream from the wing trailing edge. The computed vortex peak swirl velocities were considerably below those observed experimentally, and it was concluded that the discrepancy was caused by the inviscid model. It was also claimed that the rolled-up vortex was convected with minimal numerical diffusion. However, Strawn's[5] results predicted that the vortex core diameter increased by a factor of approximately 5 over a distance of 10 chords.

An effort to address some of the modeling and resolution difficulties inherent in earlier studies was made by Dacles-Mariani et al.[7] They obtained solutions to the full Navier–Stokes equations using the INS3D-UP code with fifth-order differencing of the convective terms for the flow about a NACA 0012 wing. A version of the one-equation Baldwin–Barth[8] turbulence model was employed in which the production term was modified in an effort to suppress the eddy viscosity in the vortex core. In a similar work, Dacles-Mariani et al.[9] used a one-equation Spalart–Almaras[10] model, again with modifications to the production term. For each study, results in terms of surface pressures and streaklines compared well with experimental data. However, prediction was limited to approximately one chord downstream of the trailing edge. Consequently, no firm conclusions can be drawn regarding the capabilities of the methodology to predict accurately the streamwise evolution of the vortex.

Hsiao and Pauley[11] investigated the tip vortex formation from a NACA 0015 rectangular wing. Their results, obtained using the INS3D-UP code and a Baldwin-Barth[8] turbulence model, were compared with the experimental data of McAlister and Takahashi[6] at a Reynolds number of 1.5×10^6 and at an angle of attack of 12 deg. Their solutions accurately captured the initial rollup of the vortex; however, they concluded that the overly dissipative nature of the turbulence model led to an excessively rapid decay of the vortex as it evolved over several chord lengths. They concluded that higher-order turbulence modeling is likely required to account for the evolution of the vortex accurately.

More recently, Lockard and Morris[12] presented higher-order solutions to the Euler equations for the evolution of the tip vortex formed over a NACA 0012 wing. Their flow conditions corresponded to those in the experimental work of Devenport et al.[13] Comparisons were made with experimental data at distances of up to nine chords downstream of the wing trailing edge. Even with the higher-order differencing, the effects of numerical dissipation were found to be quite significant on the finest H–H-type grids employed.

Results of these previous studies indicate that quantities such as surface pressure and the initial rollup of the vortex structure may be computed with good accuracy. However, the radial diffusion of angular momentum due to both insufficient grid resolution and inadequate turbulence modeling continue to represent primary impediments to the accurate prediction of tip vortices once the rollup

Received 17 April 1999; revision received 19 August 2000; accepted for publication 4 September 2000.

*Professor, Department of Mechanical and Aerospace Engineering; spall@fluids.me.usu.edu.

process is completed, typically within one to two chords downstream from the trailing edge. Past efforts at minimizing the effects of numerical dissipation have centered around the use of higher-order differencing schemes, whereas efforts in turbulence modeling have involved attempts at limiting the turbulence viscosity within the vortex core through ad hoc modifications to model production terms. It appears that little attention has been paid to methods involving the use of innovative grids and higher-order turbulence modeling.

The present work represents an effort to address the problem of excessive diffusion of the tip vortex due to numerical dissipation. Toward that end, the Euler equations are solved for the flow over a NACA 0012 rectangular wing. However, rather than following the approach of most previous investigators, which has involved the use of higher-order differencing schemes, the present work focuses on the use of computational grids that provide very high resolution of the tip vortex without excessive placement of grid points in regions where velocity gradients are small. This essentially precludes the use of simple one- and two-block H–H and C–O topologies that have been used in the past. The advantage of this approach is clear: One would like to be able to use available computational fluid dynamics (CFD) codes, the vast majority of which employ second-order accurate spatial operators, to investigate flowfields involving tip-generated vortices. In addition, Reynolds stress transport models, which are likely necessary to model accurately the effects of turbulence on the vortex structure, are simpler to implement within the context of a second-order rather than higher-order accurate framework.

The geometry considered in the present work represents that used in the experimental investigation of Devenport et al.[13] In particular, the uniform flow past a rectangular NACA 0012 wing with a rounded end cap and an aspect ratio of 8.6 is studied. When the Euler equations are solved, a computational framework is provided in which the decay of the evolving vortex may be attributed primarily to numerical dissipation. Consequently, the procedure provides an excellent means of assessing the adequacy of the grid in resolving and preserving the vortex properties as it develops in the streamwise direction. The results will show that the Euler equations are capable of predicting the strength of the tip vortex and, with a well-resolved grid, convecting the resultant vortical flow with very low numerical dissipation. The results are substantiated through comparison with experimental data presented by Devenport et al.[13]

Solution Procedure and Computational Grid

In the present work, the steady Euler equations are solved for the formation and evolution of a wing-tip vortex. The governing equations are well known, and hence for purposes of brevity are not shown (cf. White[14]). Solutions were computed using an unstructured, segregated, pressure-based finite volume procedure as implemented within the Fluent version 5.0 code. Pressure–velocity coupling within Fluent was achieved using the SIMPLEC method. Differencing of the convective terms was implemented using a third-order, bounded, QUICK interpolation scheme. Fluent employs a collocated variable scheme, and consequently the pressure must be interpolated to cell faces; this was performed using a second-order accurate interpolation scheme (cf. Barth and Jespersen[15]). Solutions were computed in parallel on a four-processor Silicon Graphics Origin 2000, with run times on the order of 24 h for grids with approximately 1×10^6 computational cells.

Although the Fluent solver employed utilizes unstructured grids, a multiblock structured grid was developed for use in this work. Multiblock structured grids have considerable potential to achieve favorable grid smoothness and orthogonality, while retaining flexibility in the gridding of complex geometries. In addition, a wide range of solvers are available that may utilize structured grids, including unstructured solvers. However, generating quality grids through the use of a large number of blocks is often the most time consuming aspect of the CFD process. To address this issue, Eiseman[16] has developed a technique that automates much of the structured grid generation process. This methodology, which is available commercially in the form of the GridPro/az3000™ grid generation package used in this work, relies primarily on the user to input the appropriate wireframe grid topology that need only roughly follow bounding surfaces. Other factors, such as surface grid generation and zone construction, are handled as part of the grid generation solution process. This procedure allows one to develop quickly quite complex multiblock grid topologies with a minimum level of user intervention. For further information the reader is referred to Refs. 16 and 17.

The computational geometry, a perspective view of which is shown in Fig. 1a, is modeled after the experimental configuration of Devenport et al.[13] (the flow direction is roughly from right to left in Fig. 1a). The x and y coordinates run in the streamwise and spanwise directions, respectively; the z coordinate runs in the vertical direction. The domain extends from $-4 \le x/c \le 13$, where $x = 0$ defines the leading edge of the NACA 0012 rectangular wing of aspect ratio 8.6 (and c is the wing chord length). The wing was fitted with a rounded end cap and set to an angle of attack of 5 deg. In addition, in accordance with the experimental conditions of Devenport et al.,[13] a uniform velocity of 38 m/s was set at the inlet of the computational domain, indicating that the flow was essentially incompressible. (The Reynolds number in the experiments was 5.3×10^5.) Zero gradient conditions were set at the outlet; slip-wall conditions were set on all other boundaries.

The most important aspect concerning the present grid involves clustering toward the vortex centerline, the trajectory of which is revealed by the ribbons trailing from the wing tip in Fig. 1a. The relevant core region is quite narrow. For instance, the experimental data[13] reveals a vortex core radius of $0.027c$ at $x/c = 10$, whereas here, and in the remainder of the paper, we use the traditional definition of the core radius: the radius at which the swirl velocity is maximum. Alternatively, Spalart[1] refers to a larger core radius, which is defined by the edge of the vorticity containing region. Using either definition, clustering efficiently to such a limited area over a significant distance in the streamwise direction is quite difficult

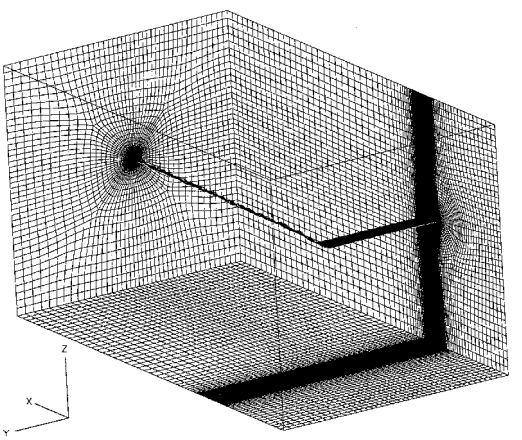

Fig. 1a Perspective view of the computational grid; 600,928 cells.

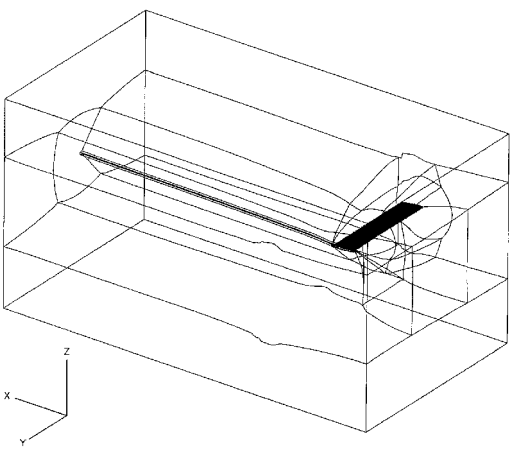

Fig. 1b Block outlines of a 12-block grid topology.

to accomplish using traditional single- or two-block H–H or C–O topologies. However, by utilizing a larger number of blocks, one may develop structured grids that are nearly orthogonal and that very efficiently cluster toward the wing-tip and vortex core regions.

Clustering about the vortex core was facilitated by the construction of a cylindrical surface, which was initiated slightly upstream of the leading outboard edge of the wing and extended to the outlet boundary. The cylinder acted as a temporary internal surface to which block boundaries were attached during the grid solution process. To locate accurately the cylinder, preliminary calculations were first performed. The resulting flowfield was then examined to identify the vortex trajectory that was subsequently assigned as the centerline of the cylinder for the construction of a grid with improved clustering. The radius of this cylinder was set to $0.25c$ over $2c \leq x \leq 13c$, gradually tapering to a radius of $0.001c$ at $x/c = -0.13$.

The grid topology about the wing surface consisted of O–O wraps in both the spanwise and chordwise directions. The number of grid points distributed around the wing surface in the chordwise direction was set to 160, with significant stretching toward the leading and trailing edges. The number in the spanwise direction varied with respect to the specific grid used; additional points resulting from refinement were clustered in the region of the wing tip. The wireframe topology implemented to develop the grid resulted in the creation of 354 elementary blocks. If necessary, these elementary blocks may then be merged to form a structured grid with as few as 12 blocks. This 12-block topological structure is shown in Fig. 1b. For use in the Fluent code, the structured grid was converted to an unstructured Nastran format. Alternatively, the grid may be output in multiblock Plot3d format directly from within the Gridpro/az3000 environment for use in structured solvers.

The primary regions of interest for the grid involve the areas surrounding the wing tip and the vortex core. An expanded view of a 600,928 cell grid in the region of the vortex at the outlet boundary is shown in Fig. 2a. The heavy grid lines correspond to elementary block boundaries; the outer radial block boundary is coincident with the aforementioned cylindrical surface, where the cylinder is of radius $0.25c$. The grid topology shown here represents an effective approach toward gridding the interior of cylindrical geometries. As already noted, the location of the cylindrical region in the y–z plane was adjusted as a function of streamwise location to ensure that the centers of the vortex and surrounding cylinder were nearly coincident. Figure 2b shows the grid in the region of the wing tip, at $x/c \approx 0.5$, where a strong clustering toward the tip region was enforced. The cylindrical region is again highlighted with the heavy grid line; at this location its radius is approximately $0.21c$.

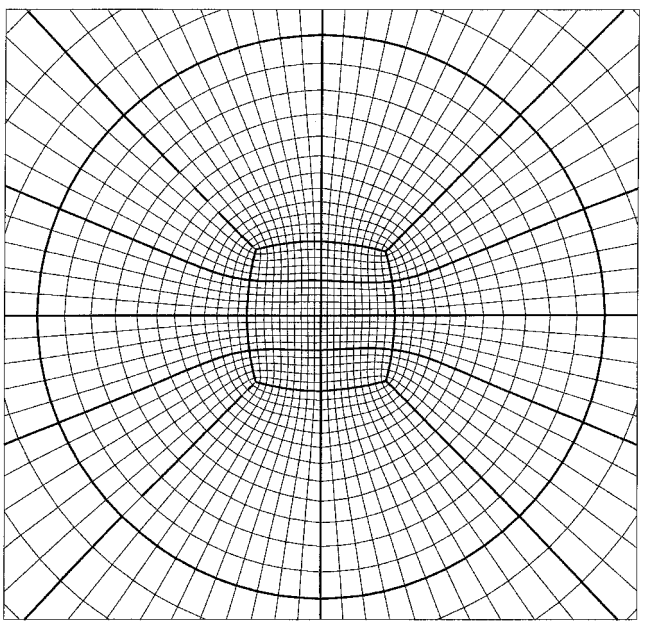

Fig. 2a Grid clustering in the region of the vortex core; 600,928 cell grid.

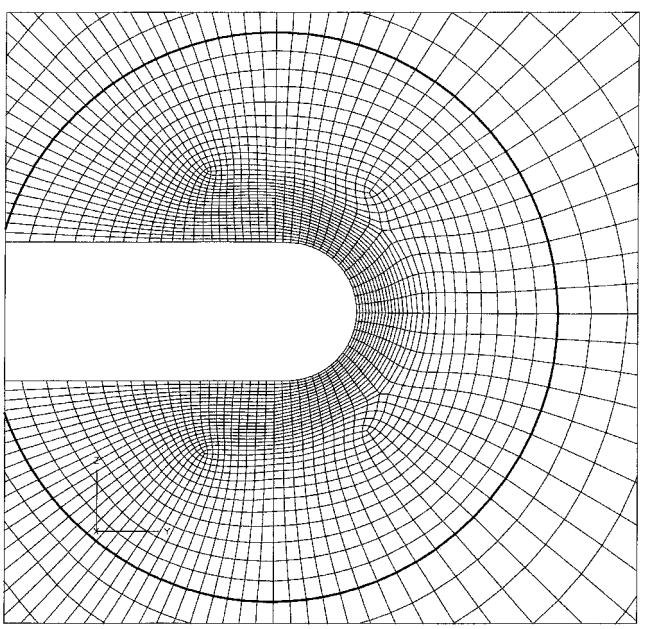

Fig. 2b Grid in the region of the wing tip; 600,928 cell grid.

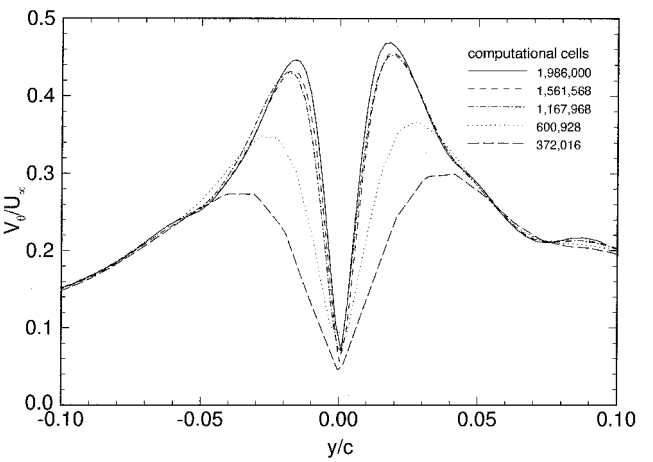

Fig. 3 Swirl velocity profiles computed using various grid resolutions at $x/c = 2.5$.

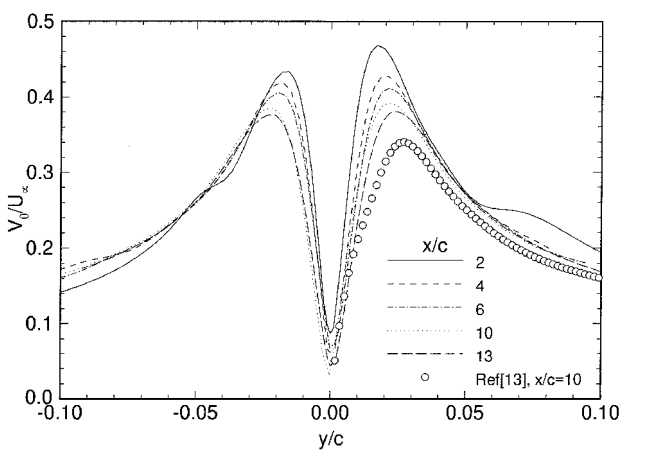

Fig. 4 Streamwise evolution of swirl velocity profiles computed using a 1,561,658 cell grid; comparison with experimental data of Devenport et al.[13] for $x/c = 10$.

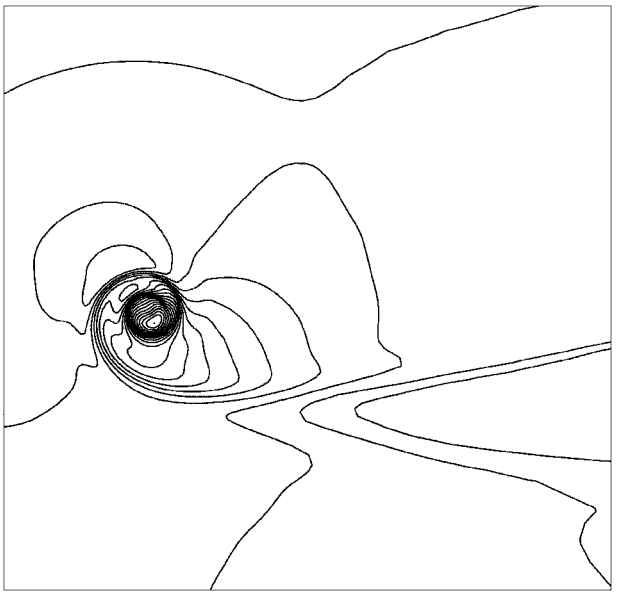

a) $x/c = 1.5$

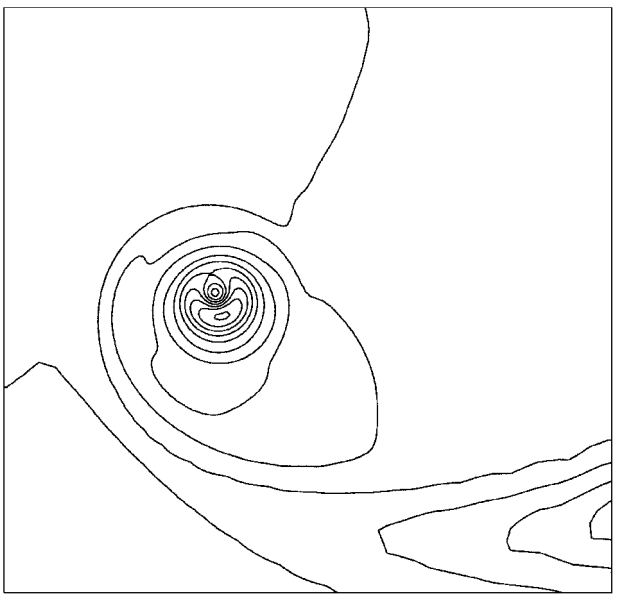

d) $x/c = 3.0$

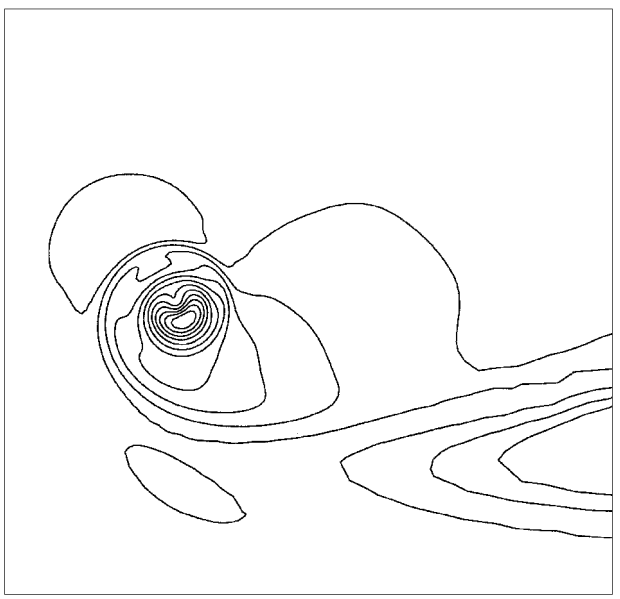

b) $x/c = 2.0$

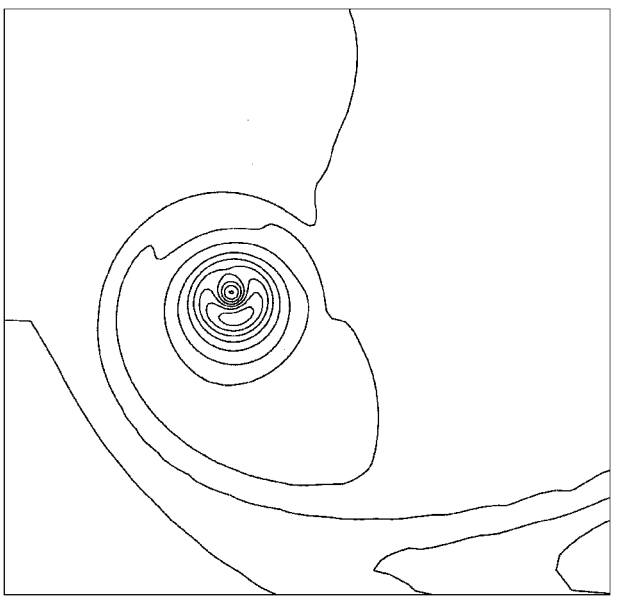

e) $x/c = 3.5$

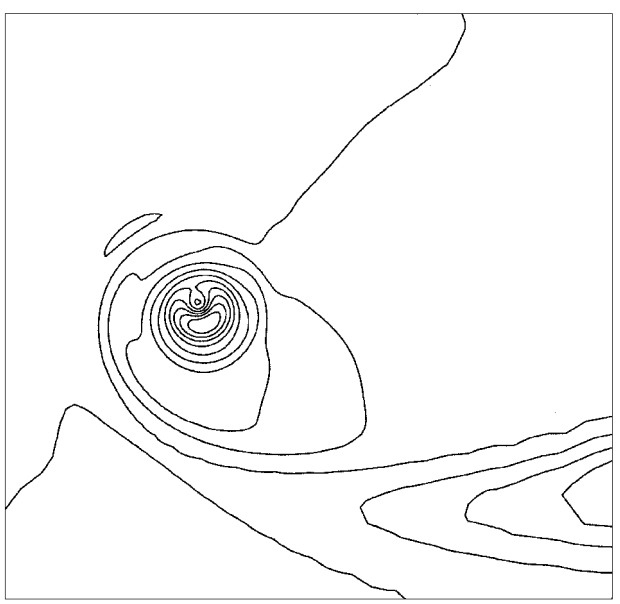

c) $x/c = 2.5$

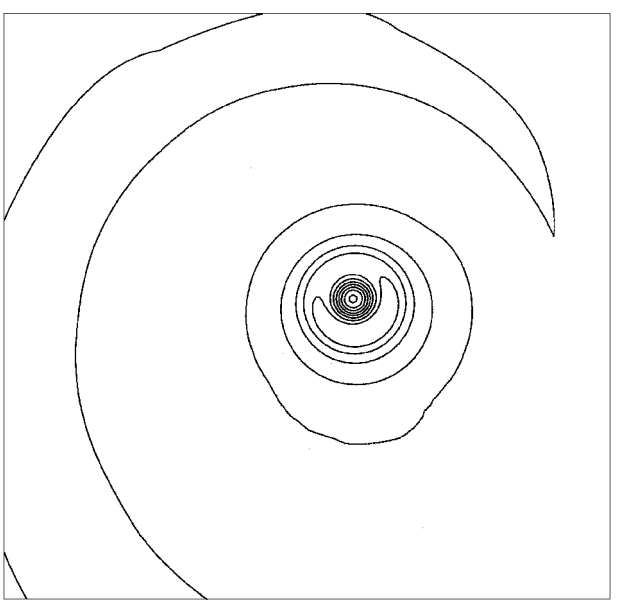

f) $x/c = 10.0$

Fig. 5 Contours of the streamwise evolution of axial velocity computed using a 1,561,658 cell grid.

Results

The results shown in Fig. 3 show the structure of the vortex as described by the swirl velocity at $x/c = 2.5$, a point at which the rollup process is essentially complete. Here, and in Figs. 4–7, unless otherwise stated y is measured relative to the center of the vortex core. In addition, the swirl velocity V_θ is measured along a line of constant z, passing through the core center. Velocity profiles are shown for grid densities ranging from 372,016 cells to 1,986,000 cells. The relatively narrow vortex core diameter of approximately $0.04c$ provides a challenge for clustering grid points. The number of cells across the core diameter ranged from 9 for the 372,016 cell case to 17 for the 1,986,000 cell case. However, one must also take into account that the core diameter for the finest grid is about half that of the 372,016 cell case; consequently, the grid spacing within the core is decreased by a factor of approximately four. The results indicate that, in terms of maximum swirl velocities and core radius, a solution that is nearly grid independent in the rollup region was achieved with approximately 1.1×10^6 computational cells. Although no experimental data are available at this particular location, results by Devenport et al.[13] for $x/c = 10$ strongly suggest that the core diameter predicted here is slightly less than that of the experiment. The circulation developed by the wing was computed by integrating the axial component of vorticity over the outlet boundary. The results showed that $\Gamma/(U_\infty b) = 0.026$ for each of the computational grids (where U_∞ is the inlet velocity and b is the wing span).

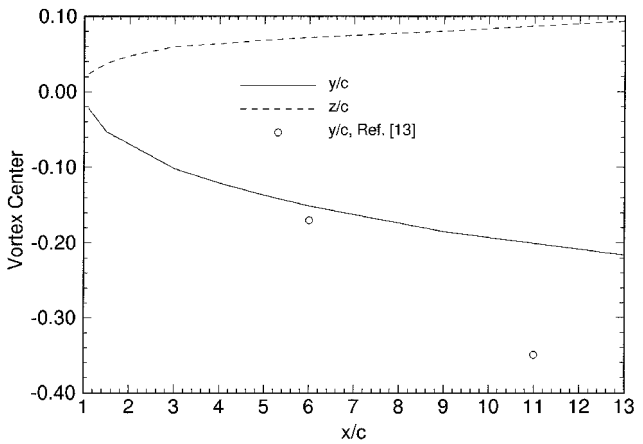

Fig. 6 Displacement of vortex core referenced to y, z coordinate position of vortex center at x/c = 1.1.

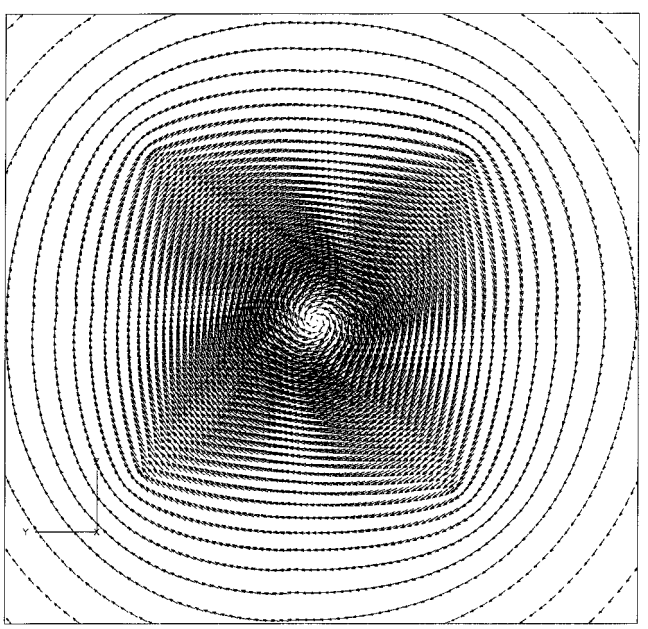

Fig. 7 Velocity vectors at x/c = 10 for the 1,561,658 cell grid revealing the position of the vortex within the region of clustering.

Once the initial vortex structure is established, solutions to the Euler equations may be quite valuable in assessing the levels and/or effects of numerical dissipation as the vortex evolves in the streamwise direction. In the absence of viscous effects, the core radius and peak swirl velocity of the evolving vortex should remain nearly constant. Such an evaluation of the inviscid solution is shown in Fig. 4 for the case employing 1,561,568 computational cells. Experimental data of Devenport et al.[13] for $x/c = 10$ is also included in Fig. 4. (For the rounded end-cap case, experimental data are available at this location only. Detailed comparisons with flat end-cap data are probably not useful; for instance, the results of Devenport et al. revealed that, relative to the rounded end cap, use of a flat end cap increased the core diameter at $x/c = 10$, by approximately 37%.) The numerical results indicate an asymmetry in the vortex at $x/c = 2$ with the lower of the peaks occurring on the inboard side. This is likely due to interference from the wing. This asymmetry has been essentially eliminated at $x/c = 4$, primarily through a decrease in the swirl velocity in the outboard region of the vortex. Subsequently, peak swirl velocities decay relatively slowly, and the core diameter increases only slightly over the range $4 \leq x/c \leq 13$. At $x/c = 10$, the predicted core radius is less than, and the peak swirl velocity greater than, the respective experimental values. Specifically, the experimental value of the core radius was $0.027c$, whereas the predicted value was approximately $0.021c$. To achieve these results, 14 computational cells were distributed over the core diameter at $x/c = 2$, increasing to 18 cells at $x/c = 10$. These results may be contrasted with the inviscid solution computed using a higher-order solver presented by Lockard and Morris[11] for the same configuration, where the predicted vortex core radius increased from approximately $0.07c$ at $x/c = 2.5$ to $0.155c$ at $x/c = 10$. That solution employed a two-block H–H grid with a total of 1.955×10^6 grid points.

Contours of constant axial velocity are examined in Figs. 5a–5f at streamwise locations $x/c = 1.5$, 2, 2.5, 3, 3.5, and 10, respectively. The contours at $x/c = 1.5$ reveal the existence of a jet that is near, but not coincident with, the center of the vortex. At this point, the velocity excess at the center of the jet is $(U - U_\infty)/U_\infty = 0.10$. As the vortex evolves in the streamwise direction, the jet begins to wrap around a developing wake region. The developing wake profile does, in fact, coincide with the center of the vortex. This process is clearly shown in Figs. 5c–5e. At $x/c = 10$, the axial velocity distribution around the core has become nearly symmetric with defect $(U - U_\infty)/U_\infty = -0.012$ at the center of the vortex. The wake is surrounded by an annular jetlike region with peak value $(U - U_\infty)/U_\infty = 0.029$ at $y/c = 0.028$. This location is quite close to the vortex core radius of $0.021c$. The magnitude of the defect within the wake is, however, considerably less than that in the experiment,[13] where $(U - U_\infty)/U_\infty = -0.19$. In addition, the annular jetlike profile surrounding the core found in the numerical results was not observed in the experiments.

The displacement of the vortex core as it evolves in the streamwise direction is shown in Fig. 6, where the location of the vortex has been referenced to the location of the wing tip at $y = 4.3$, $z = 0.0$. Experimental data of Devenport et al.[13] (however, with a flat end cap) is included in Fig. 6 for the spanwise movement of the vortex. Good agreement is obtained at $x/c = 6$; however, the experiment shows much greater spanwise deflection at $x/c = 11$. Experimental data for the vertical movement have not been included in Fig. 6 due to difficulties in referencing the vortex location with respect to the wing tip. Nevertheless, the motion of the core in the z direction as determined by Devenport et al. was upward, with an absolute displacement of approximately 0.1 over the range $6 \leq x/c \leq 11$. This vertical movement is greater than that observed in the calculation. Lockard and Morris[12] observed qualitatively similar behavior when comparing their numerical results with the results of Devenport et al.[13]

To minimize numerical dissipation, the computational cells must be clustered about the quite narrow region of the vortex core. Calculations revealed that a slight displacement of the vortex outside the cluster region leads to considerable degradation of the results.

The velocity vectors shown in Fig. 7 indicate the placement of the vortex within the cluster for the 1,561,568 cell grid at $x/c = 10$, where the diameter of the computational domain shown in Fig. 7 is approximately $0.23c$. This clustering may be quite easily extended arbitrary distances downstream.

The inviscid calculations do not account for the effect of the no-slip surface, and the source of diffusion over the interior of the fluid is solely due to truncation error. Consequently, the solutions can not be expected to provide accurate information regarding the detailed structure of the rolled-up tip vortex. Nevertheless, the results presented have shown that solutions to the Euler equations may provide an excellent estimate of the vortex core diameter and associated peak swirl velocities for up to 12 chords downstream of the wing trailing edge. Discrepancies with experimental results in the axial velocity profiles are greater and may well be attributed to the lack of a no-slip condition on the wing surface.

Summary

Using a second-order-accurate procedure, solutions to the Euler equations were obtained for the evolution of a wing-tip vortex over a streamwise distance of 13 chords. By clustering grid points strongly in the vortex core, results were obtained that did not suffer from the extensive effects of numerical dissipation common in calculations of this type. In fact, with sufficiently fine grids, the vortex core radius predicted by the Euler solutions was smaller than that observed experimentally. The corresponding peak swirl velocities also exceeded the experimental values. The author is not aware of any other published studies where this behavior has been demonstrated. However, this result is not surprising considering the inviscid and, hence, nondissipative nature of the equations, and the low levels of numerical dissipation associated with a very fine grid in the tip and core regions. Extending the computational domain to arbitrary x/c with accurate clustering about the vortex centerline poses no additional problems.

In summary, the procedure presented presents a viable alternative to using higher-order numerical methods for the solution of the tip vortex problem. The work also represents an important first step before performing calculations of tip vortex flows using Reynolds-averaged Navier–Stokes formulations in that guidance is provided in terms of minimum required grid resolution for the viscous case, where to predict accurately the vortex structure, the levels of numerical viscosity should be small relative to the natural viscosity.

Acknowledgments

This work has been funded through NASA Langley Research Center under Grant NAG1-1871. Peter Eisman of Program Development Corporation is gratefully acknowledged for providing the prototype grid topology. Warren Phillips is thanked for sharing his insight with the author.

References

[1]Spalart, P. R., "Airplane Trailing Vortices," *Annual Review of Fluid Mechanics*, Vol. 30, pp. 107–138.

[2]Mansour, N. N., "Numerical Simulation of the Tip Vortex Off a Low-Aspect Ratio Wing at Transonic Speed," *AIAA Journal*, Vol. 23, No. 8, 1985, pp. 1143–1149.

[3]Srinivasan, G. R., McCroskey, W. J., Baeder, J. D., and Edwards, T. A., "Numerical Simulation of Tip Vortices of Wings in Subsonic and Transonic Flows," *AIAA Journal*, Vol. 26, No. 10, 1988, pp. 1153–1162.

[4]Kramer, E., Hertel, J., and Wagner, S., "Computation of Subsonic and Transonic Helicopter Rotor Flow Using Euler Equations," *Vertica*, Vol. 12, No. 3, 1988, pp. 279–291.

[5]Strawn, R. C., "Wing Tip Vortex Calculations with an Unstructured Adaptive-Grid Euler Solver," 47th Annual Forum of the American Helicopter Society, Phoenix, AZ, May 1991.

[6]McAlister, K. W., and Takahashi, R. K., "NACA 0015 Wing Pressure and Trailing Vortex Measurements," NASA TP 3151, 1991.

[7]Dacles-Mariani, J. S., Zilliac, G. G., Chow, J. S., and Bradshaw, P., "Numerical/Experimental Study of a Wingtip Vortex in the Near Field," *AIAA Journal*, Vol. 33, No. 9, 1995, pp. 1561–1568.

[8]Baldwin, B. S., and Barth, T. J., "A One-Equation Transport Model for High Reynolds Number Wall-Bounded Flows," NASA TM 102847, 1990.

[9]Dacles-Mariani, J. S., Kwak, D., and Zilliac, G., "Accuracy Assessment of a Wingtip Vortex Flowfield in the Near-Field Region," AIAA Paper 96-0208, Jan. 1996.

[10]Spalart, P. R., and Allmaras, S. R., "A One-Equation Turbulence Model for Aerodynamic Flows," *La Recherche Aerospatiale*, 1994-1, 1994, pp. 5–21.

[11]Hsiao, C.-T., and Pauley, L. L., "Numerical Study of the Steady-State Tip Vortex Flow Over a Finite-Span Hydrofoil," *ASME Journal of Fluids Engineering*, Vol. 120, No. 6, 1998, pp. 345–353.

[12]Lockard, D. P., and Morris, P. J., "Wing-Tip Vortex Calculations Using a High-Accuracy Scheme," *Journal of Aircraft*, Vol. 35, No. 5, 1998, pp. 728–738.

[13]Devenport, W. J., Rife, M. C., Liapis, S. I., and Follin, G. J., "The Structure and Development of a Wing-Tip Vortex," *Journal of Fluid Mechanics*, Vol. 312, 1996, pp. 67–106.

[14]White, F. M., *Viscous Fluid Flow*, 2nd ed., McGraw–Hill, New York, 1994, p. 73.

[15]Barth, T. J., and Jespersen, D., "The Design and Application of Upwind Schemes on Unstructured Meshes," AIAA Paper 89-0366, Jan. 1989.

[16]Eiseman, P. R., "Automatic Structured Grid Generation," *Computational Fluid Dynamics Review*, edited by M. Hafez, and K. Oshima, Wiley, U.K., 1995.

[17]Cheng, Z., and Eiseman, P. R., "Interactive Topology Generation and Grid Viewer for GridPro/az3000," *Proceedings of the 5th International Conference on Numerical Grid Generation in CFD*, 1–5 April 1996.